

Observation of a novel orbital selective Mott transition in $\text{Ca}_{1.8}\text{Sr}_{0.2}\text{RuO}_4$

M. Neupane,¹ P. Richard,^{1,2} Z.-H. Pan,¹ Y. Xu,¹ R. Jin,³ D.
Mandrus,³ X. Dai,⁴ Z. Fang,⁴ Z. Wang,¹ and H. Ding^{1,4,*}

¹*Department of Physics, Boston College, Chestnut Hill, MA 02467, USA*

²*WPI-AIMR, Tohoku University, Sendai 980-8578, Japan*

³*Condensed Matter Science Division,*

Oak Ridge National Laboratory, Oak Ridge, Tennessee 37831, USA

⁴*Beijing National Laboratory for Condensed Matter Physics,
and Institute of Physics, Chinese Academy of Sciences, Beijing 100190, China*

(Dated: August 20, 2021)

*Electronic address: dingh@bc.edu

Electrons in a simple correlated system behave either as itinerant charge carriers or as localized moments. However, there is growing evidence for the coexistence of itinerant electrons and local moments in transition metals with nearly degenerate d -orbitals. It demands one or more selective electron orbitals undergo the Mott transition while the others remain itinerant. Here we report the first observation of such an orbital selective Mott transition (OSMT) in $\text{Ca}_{1.8}\text{Sr}_{0.2}\text{RuO}_4$ by angle-resolved photoemission spectroscopy (ARPES). While we observed two sets of dispersing bands and Fermi surface associated with the doubly-degenerate d_{yz} and d_{zx} orbitals, the Fermi surface associated with the wider d_{xy} band is missing, a consequence of selective Mott localization. Our theoretical calculations demonstrate that this novel OSMT is mainly driven by the combined effects of interorbital carrier transfer, superlattice potential, and orbital degeneracy, whereas the bandwidth difference plays a less important role.

$\text{Ca}_{2-x}\text{Sr}_x\text{RuO}_4$ is a fascinating $4d$ multi-orbital system that exhibits a rich and intricate phase diagram, ranging from a chiral p -wave superconductor (Sr_2RuO_4) to a Mott insulator (Ca_2RuO_4) [1, 2]. Similar to the high- T_c cuprates, the metal-insulator transition under the influence of electron correlations in the ruthenates is of fundamental importance and currently under intensive debate. There is accumulating experimental evidence for coexistence of local moments and metallic transport, and heavy fermion behavior in the region of $0.2 \leq x \leq 0.5$ [2, 3, 4], which is remarkable because there are no f -electrons in this material. To account for the coexistence of localized and itinerant electrons in this region, a scenario of OSMT has been proposed [5, 6] as following: Sr_2RuO_4 has three degenerated t_{2g} orbitals (d_{xy} , d_{yz} , and d_{zx}) occupied by four $4d$ electrons. The isovalent Ca substitute does not change the total carrier concentration (i.e. no doping), but rather increases the effective electron correlation strength (U_{eff}) relative to the reduced bandwidth which is induced by structural change due to the smaller Ca^{2+} ion radius. Consequently, it is possible that an OSMT takes place in the narrower bands, i.e., the one-dimensional (1D) d_{yz} and d_{zx} orbitals, where electrons undergo a Mott transition and become localized, while the electrons in the wider two-dimensional (2D) d_{xy} band remain itinerant. A similar partial localization mechanism has been proposed for some heavy fermion materials, e. g., UPd_2Al_3 [7].

While the concept of OSMT is of critical importance to the multi-orbital Mott Hubbard

systems and has been studied extensively in theory [5, 6, 8, 9, 10], it has not been confirmed experimentally. Our previous ARPES [11] shows that, for samples with $x = 0.5$, the two 1D (α and β) Fermi surface (FS) sheets are clearly “visible”. The 2D (γ) FS, while being heavily smeared, survives at this substitution level. This is in sharp contrast to the OSMT prediction that the 1D FS sheets become Mott localized. To check if the OSMT occurs at a lower Sr concentration, we have conducted a series of ARPES experiments on high-quality single crystals at $x = 0.2$, grown by the floating zone technique [4]. Precise determination of the low-energy electronic structure at this doping level is important since $\text{Ca}_{1.8}\text{Sr}_{0.2}\text{RuO}_4$ is at the boundary between a magnetic metal and an antiferromagnetic insulator, and exhibits non-Fermi liquid behaviors in the resistivity [2]. However, it is a rather difficult and lengthy experiment due to a much reduced ARPES spectral intensity in the vicinity of the Fermi energy (E_F) near the insulating phase. Several techniques have been used to boost photoelectron signals, including enhancement of the APRES matrix elements through fine tuning of photon energy and measurements at different Broullion zones (BZs).

As shown in Fig. 1, strong spectral intensity and clear dispersion are observed in the valence bands of $\text{Ca}_{1.8}\text{Sr}_{0.2}\text{RuO}_4$, similar to the case of Sr_2RuO_4 , indicating good quality of sample and surface. However, the spectral intensity near E_F experiences dramatic reductions as the Sr content x approaches 0.2, as demonstrated in Fig. 1c, reflecting the fact that the system is near an insulating phase. To see clearly the low-energy excitations, we zoom in to the binding energy range within 0.2 eV of E_F , as plotted in Fig. 2. One can identify weak but discernible peaks dispersing towards to E_F , as shown in Figs. 2c and d. More specifically, we observe, as illustrated in Figs. 2a and b, two linearly dispersive bands along the high-symmetry line $X\text{-}\Gamma\text{-}X$, or $(\pi, \pi)\text{-(0,0)-}(-\pi, -\pi)$, crossing E_F around 0.3 and -0.9 \AA^{-1} , respectively. These two Fermi crossing (k_F) points, plotted in Fig. 2f as points # 1 and 2, locate on the calculated α Fermi surface for Sr_2RuO_4 and its folded FS (labeled as the α' FS) due to the $\sqrt{2} \times \sqrt{2}$ reconstruction caused by a rotation of the RuO_6 octahedra [12]. We note that the peak intensity in both energy distribution curves (EDCs) and momentum distribution curves (MDCs) diminishes as it approaches E_F or k_F , possibly due to a small energy gap or the quasiparticle decoherence effect observed in some transition metal oxides near the metal-insulator boundary [13]. The band dispersion along another high-symmetry line $M\text{-}\Gamma\text{-}M$ is displayed in Fig. 2E, and we observed four FS crossings (points #3 - #6) whose locations are plotted in Fig. 2F. While the crossing points #4 and 5 are on the

calculated α' FS, and #3 and 6 are close to the β FS, there is no observation of the dispersing γ band and the corresponding FS crossing.

To verify these band and FS assignments, we have performed many measurements to cover a wide range of k-space. We locate and plot all observed FS crossing points in the first BZ shown in Fig. 3a. It is clear that both the α and β main FS sheets and the folded α' FS are present in $\text{Ca}_{1.8}\text{Sr}_{0.2}\text{RuO}_4$. However, no evidence of the γ FS is found. The disappearance of the γ FS is very puzzling. According to Luttinger counting theorem, the total occupied FS area should remain the same due to the isovalence nature of the Ca-Sr substitution. From the fitted α and β FS sheets, as shown in Fig. 3a, we derive the electron occupations $n_\alpha = 1.72$ and $n_\beta = 0.74$, implying that the γ band has 1.52 valence electrons since $n_{total} = 4$. To illustrate this point, in Fig. 3a we plot the “would be” γ FS as a simple circle (black dashed line), which satisfies the Luttinger counting of 1.52 electrons. Note that it would almost touch the M ($\pi, 0$) point, indicating that its van Hove singularity is very close to the Fermi energy, which may lead to instability at low temperature.

To further understand the fate of the γ band, we plot in Fig. 3b an EDC of $\text{Ca}_{1.8}\text{Sr}_{0.2}\text{RuO}_4$ integrated over the neighboring region of M (indicated by a rectangular box around M in Fig. 3a). In contrast to the EDC of Sr_2RuO_4 at M , which is also plotted in Fig. 3b, the EDC of $\text{Ca}_{1.8}\text{Sr}_{0.2}\text{RuO}_4$ shows a dramatic suppression of the γ quasiparticles (QPs). In fact, the spectrum consists of a broad feature with a gap of $\gtrsim 100$ meV, and a small “foot” extending toward E_F . The origin of this small “foot” is not entirely clear, although it may possibly come from a residual γ band from a minority phase, or certain impurity states. We regard the disappearance of the γ QP with a large soft gap as an evidence for possible localization of the γ band. We notice that the electron occupancy of the γ band is close to 1.5 (a half integer) from both the experimental derivation based on Luttinger theorem as discussed above, and our theoretical calculation using local density approximation (LDA), as shown in Fig. 3c. It is remarkable that the LDA calculation shows good agreement with the ARPES experimental observation. The basic reason for the increase of the γ electron occupation is that the increased hybridization between the t_{2g} and e_g orbitals, due to the increasing rotation and tilting of octahedra at higher Ca content, pushes down the d_{xy} band. The same effect has been also observed in a similar 4d-electron system (Sr_2RhO_4) [14].

A natural question is why the FS and the coherent excitations from the γ band are absent at 1.5 electron occupancy. Remarkably, as the system undergoes the $\sqrt{2} \times \sqrt{2}$ reconstruc-

tion in the bulk [12], the γ band folds into two subbands by the superlattice potential, accompanied by the doubling of the unit cell. The folded γ bands in the reduced Brillouin zone host a total of 3 electrons. The lower subband is completely filled while the upper one is precisely at half-filling. It is thus possible for the γ -complex to undergo the Mott transition and become localized, contributing a spin-1/2 local moment. Since there are two Ru atoms per supercell, the localized magnetic moment is $0.5 \mu_B$ per Ru atom. This is indeed consistent with the field dependent magnetization measurement in $\text{Ca}_{1.8}\text{Sr}_{0.2}\text{RuO}_4$ [3]. The sharp increase of the magnetization to $0.5 \mu_B$ as the applied magnetic field reaches about 5T can be attributed naturally to the polarization of the local moment, whereas the subsequent gradual growth of the magnetization with further increasing field arises from Pauli paramagnetism of the itinerant α and β band electrons.

Theoretically, most of the model studies have focused on the two-band Hubbard model, where the OSMT is mainly controlled by the difference in the bandwidths [6, 8]. The real situation in $\text{Ca}_{2-x}\text{Sr}_x\text{RuO}_4$ system is more complex. Due to the $\sqrt{2} \times \sqrt{2}$ super structure, there is a total of six bands occupied by eight electrons in the doubled unit cell. We have carried out first-principle calculations and found that the lower three bonding bands are fully occupied by six electrons. The remaining two electrons occupy the upper three anti-bonding bands. If there were no crystal field splitting, these two electrons would be almost evenly distributed among the upper three bands, corresponding to occupations (2/3, 2/3, 2/3). However, the localized orbital must be filled by an odd integer number of electrons in an OSMT, which can be realized in $\text{Ca}_{2-x}\text{Sr}_x\text{RuO}_4$ only when the two electrons redistribute among the upper three bands to reach occupations (1/2, 1/2, 1) due to the crystal field splitting. This is consistent with our ARPES measurements near $x = 0.2$. Indeed, our LDA calculation shows that, with the reduction of the Sr concentration x , the crystal field pulls down the γ band and transfers charge from the α , β bands to the γ band as shown in Fig. 3c. When the electron distribution reaches (1/2, 1/2, 1), the three-band complex splits into two groups: two nearly degenerate α and β bands, and a separated γ band with a lowered center of gravity. Therefore, we have one two-band system and one single band system, both with one electron per unit cell. The reason for the OSMT to take place in the γ band is that the critical interaction U_c for the Mott transition in a single band Hubbard model is about 30% smaller than that of a two-band model with one electron per unit cell and identical bandwidth, a result obtained by variational Gutzwiller and dy-

namical meanfield theory [16]. The Hund's rule coupling further increases the critical U_c for the two-band system. Therefore, in a large area of the parameter space, the single γ -band system lies in the Mott phase contributing the local moment, while the two-band system remains in the metallic phase contributing itinerant electrons.

To further illustrate this point, we apply the slave boson mean field theory to a simple three-band Hubbard model with the bandwidth ratios of 1:1:1 and 1:1:1.5 and two electrons per unit cell. The technical details have been explained in reference [17]. In Fig. 4, we plot the quasiparticle coherence weight (Z) and the orbital correlations as a function of the charge transfer δ . Fig. 4a clearly shows that the coherence weight of the γ band decreases continuously while that of the degenerate α band remains almost a constant as the OSMT is approached at charge transfer $\delta = 1/3$, which corresponds to the charge distribution $(1/2, 1/2, 1)$. Concomitantly, as can be seen from Fig. 4b, the inter-band correlations (χ) between the γ and the α, β bands are dramatically reduced. To verify that the bandwidth difference does not play an important role in the OSMT, we show in Figs. 4c and 4d that the same conclusion is reached for the case where the γ band is 1.5 times as wide as that of the α and β bands.

In conclusion, we have successfully measured the low energy excitations in multi orbital ruthenate $Ca_{2-x}Sr_xRuO_4$ near $x = 0.2$ by ARPES and unraveled a novel mechanism for the OSMT. The low-energy band dispersions and the associated FS are observed for the d_{yz} and d_{zx} orbitals. In contrast, the d_{xy} orbital shows a loss of coherent low energy quasiparticle excitations due to Mott localization. We discovered that the $\sqrt{2} \times \sqrt{2}$ structure reconstruction plays a crucial role in establishing the half-filling condition of the anti-bonding γ band. We provided microscopic theoretical support for this novel OSMT and demonstrated the importance of the crystal field splitting induced interorbital charge transfer and the orbital degeneracy for promoting an intriguing electronic phase with coexisting local moment and itinerant electrons. Our findings highlight the emergent and fundamentally important phenomena governed by the Mott physics in multi-orbital correlated electron systems, and call for more systematic studies of transition metal based materials.

METHODS

All of our experiments have been performed at high-flux synchrotron undulator beam lines (e.g., Wadsworth,U1-NIM,PGM at the Synchrotron Radiation Center, Wisconsin), using a high-efficiency Scienta SES-2002 electron analyzer. The energy and momentum resolutions are 10 - 30 meV and 0.02 \AA^{-1} , respectively. Samples were cleaved *in situ* and measured at 40 K in a vacuum better than 1×10^{-10} torr. The samples have been found to be very stable and without degradation for the typical measurement period of 48 hours.

References

-
- [1] Maeno Y. *et al.* Superconductivity in a layered perovskite without copper. *Nature* **372**, 532-534 (1994).
 - [2] Nakatsuji, S. & Maeno,Y. Quasi-two dimensional Mott transition system $\text{Ca}_{2-x}\text{Sr}_x\text{RuO}_4$. *Phys. Rev. Lett.* **84**, 2666-2669 (2000).
 - [3] Nakatsuji, S. *et al.* Heavy-mass Fermi liquid near a ferromagnetic instability in layered ruthenates. *Phys. Rev. Lett.* **90**, 137202 (2003).
 - [4] Jin, R. *et al.* Heavy-electron behavior and structural change in $\text{Ca}_{1.7}\text{Sr}_{0.3}\text{RuO}_4$. Preprint at <http://arxiv.org/abs/Cond-mat/0112405> (2001).
 - [5] Anisimov, V. I. *et al.* Orbital-selective Mott-insulator transition in $\text{Ca}_{2-x}\text{Sr}_x\text{RuO}_4$. *Eur. Phys. J. B* **25**, 191 (2002).
 - [6] Koga, A. *et al.* Orbital-selective Mott transitions in the degenerate Hubbard model. *Phys. Rev. Lett.* **92**, 216402 (2004).
 - [7] Sato, N. *et al.* Strong coupling between local moments and superconducting heavy electrons in UPd_2Al_3 . *Nature* **410**, 340-343 (2001).
 - [8] Liebsch, A. Mott transitions in multiorbital systems. *Phys. Rev. Lett.* **91**, 226401 (2003).
 - [9] Liebsch, A. Subband filling and Mott transition in $\text{Ca}_{2-x}\text{Sr}_x\text{RuO}_4$. *Phys. Rev. Lett.* **98**, 216403 (2007).
 - [10] Fang, Z., Nagaosa, N. & Terakura, K. Orbital-dependent phase control in $\text{Ca}_{2-x}\text{Sr}_x\text{RuO}_4$ ($0 \leq$

- $x \leq 0.5$). *Phys. Rev. B* **69**, 045116 (2004).
- [11] Wang S.-C. *et al.*, Fermi surface topology of $\text{Ca}_{1.8}\text{Sr}_{0.2}\text{RuO}_4$ determined by angle-resolved photoelectron spectroscopy. *Phys. Rev. Lett.* **93**, 177007 (2004).
 - [12] Matzdorf, R. *et al.* Ferromagnetism stabilized by lattice distortion at the surface of the p-wave superconductor Sr_2RuO_4 . *Science* **289**, 746 (2000).
 - [13] Dessau, D. S. *et al.* k-dependent electronic structure, a large "ghost" Fermi surface, and a pseudogap in a layered magnetoresistive oxide. *Phys. Rev. Lett.* **81**, 192 (1998).
 - [14] Kim, B. J. *et al.* Missing xy-band Fermi surface in 4d transition-metal oxide *Phys. Rev. Lett.* **97**, 106401 (2006).
 - [15] Oguchi, T. *et al.* Electronic band structure of the superconductor Sr_2RuO_4 . *Phys. Rev. B* **51**, 1385 (1995).
 - [16] Florens, S., Georges, A., Kotliar, G. & Parcollet, O. Mott transition at large orbital degeneracy: Dynamical mean-field theory. *Phys. Rev. B* **66**, 205102 (2002); Lu J. P. Metal-insulator transitions in degenerate Hubbard models and A_xC_{60} . *Phys. Rev. B* **49**, 5687 (1994).
 - [17] Dai, X., Kotliar, G., & Fang, Z. The orbital selective Mott transition in a three band Hubbard model: a slave Boson mean field study. Preprint at < <http://arxiv.org/abs/Cond-mat/0611075>> (2006).

Acknowledgments

This work was supported by grants of US NSF DMR-0353108, DMR-0704545, US DOE DEFG02-99ER45747, and China NSF. This work is based upon research conducted at the Synchrotron Radiation Center supported by NSF DMR-0537588. Oak Ridge National laboratory is managed by UT-Battelle, LLC, for DOE under contract DE-AC05-00OR22725.

Author information

Correspondence and requests for materials should be addressed to H.D.

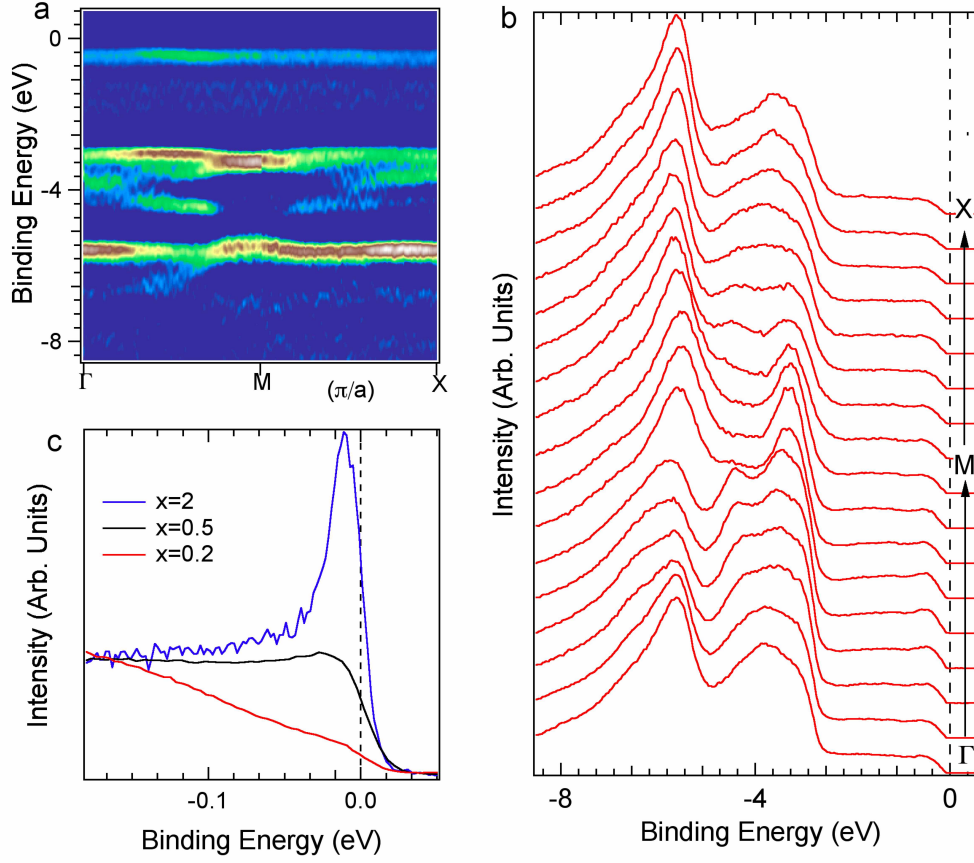


FIG. 1: **Valence bands of $\text{Ca}_{1.8}\text{Sr}_{0.2}\text{RuO}_4$.** (a) Plot of second derivative of ARPES intensity for the valence band of $\text{Ca}_{1.8}\text{Sr}_{0.2}\text{RuO}_4$ taken along Γ -M-X ($h\nu = 75$ eV, $T = 40$ K). (b) The corresponding EDCs along Γ -M-X. (c) Comparison of the EDCs for $x = 0.2, 0.5, 2$, taken at the β band crossing point along Γ -M ($h\nu = 32$ eV, $T = 40$ K)

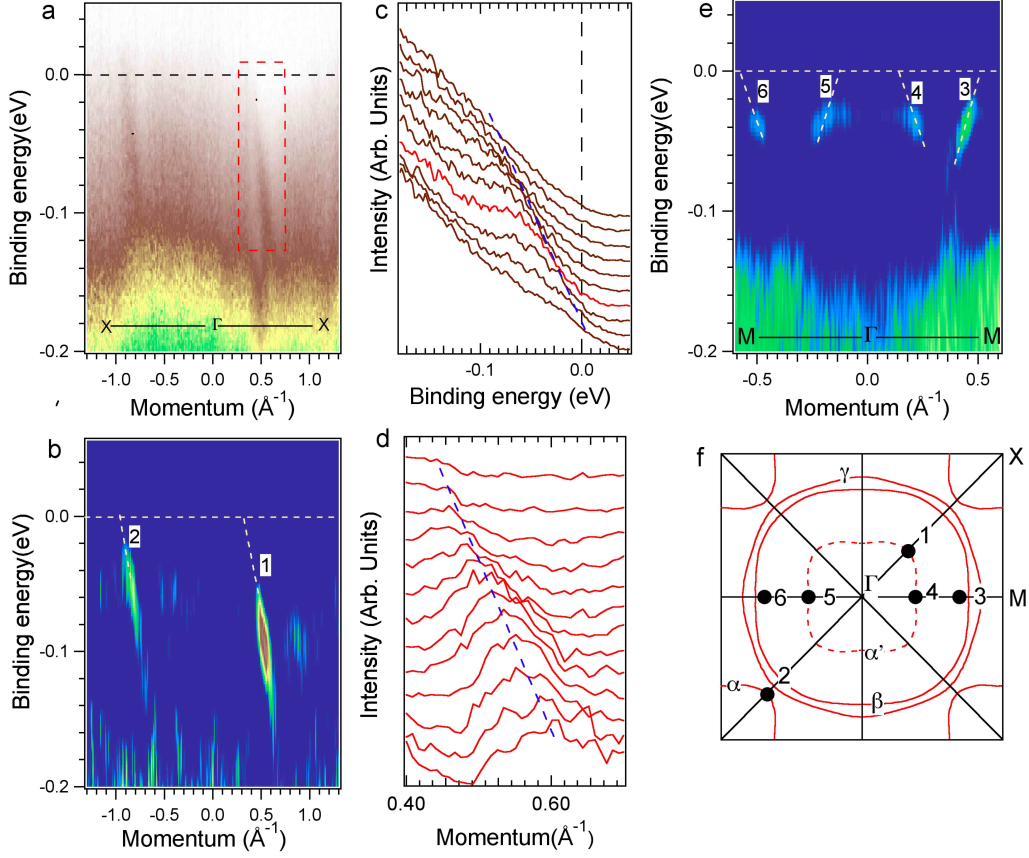


FIG. 2: **Band dispersion along high-symmetry directions in $\text{Ca}_{1.8}\text{Sr}_{0.2}\text{RuO}_4$.** (a) ARPES intensity plot along $X-\Gamma-X$. (b) The corresponding second derivative plot of (a). The white dashed lines are linear extrapolations for the band dispersion. (c) EDCs, and (d) MDCs, within the red dashed box in (A), showing low-energy band dispersion, as indicated by blue dashed lines. (e) Second derivative plot of ARPES intensity along $M-\Gamma-M$. (f) Fermi crossings (black dots) indicated in (b) and (e), and Fermi surface sheets (red lines) calculated by LDA for Sr_2RuO_4 [15] in the first BZ.

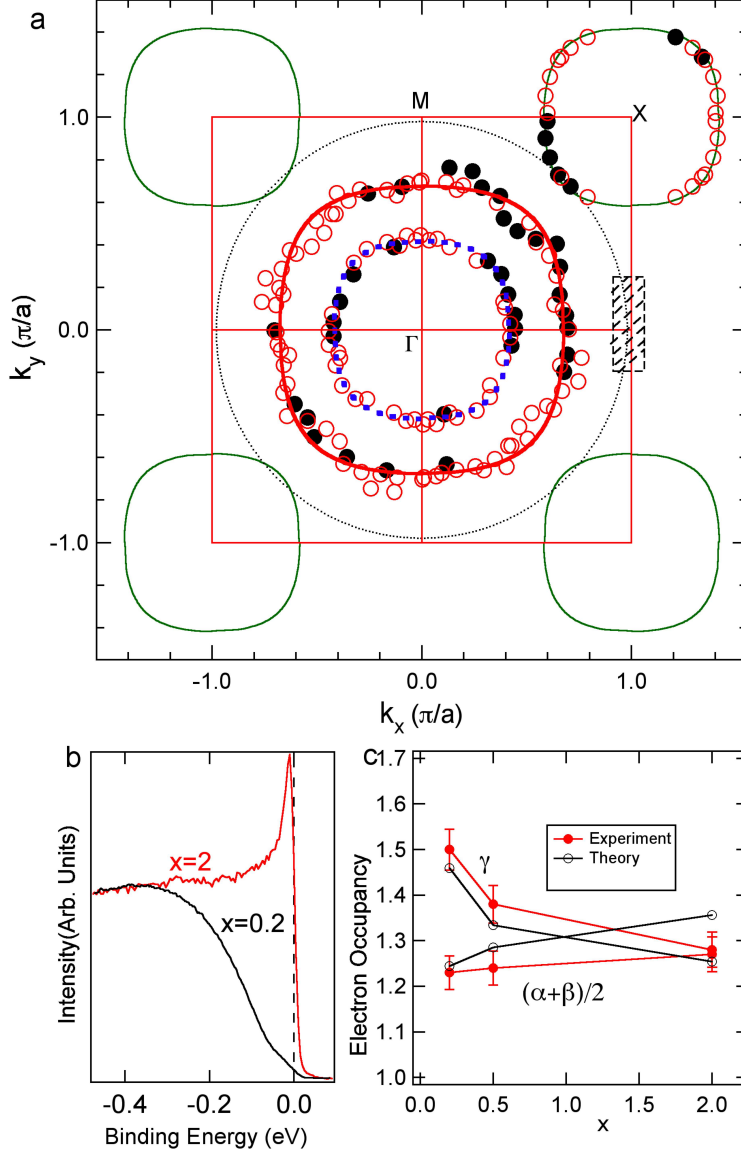


FIG. 3: **Fermi surface and electron occupancy of different orbitals.** (a) Measured Fermi surface sheets of α (green contours centered at X), β (red contour centered at Γ), and the folded α (blue dashed contour centered at Γ), along with the Fermi crossing points determined by ARPES measurements (black solid dots) and symmetrized points according to the 4-fold crystal symmetry (red open dots). The black dotted contour centered at Γ is the derived γ Fermi surface according to Luttinger counting theorem. (b) Comparison of the $(\pi, 0)$ EDCs between $\text{Ca}_{1.8}\text{Sr}_{0.2}\text{RuO}_4$ and Sr_2RuO_4 , integrated over the k -region indicated by the shaded rectangle in (a). (c) The Sr content dependence of electron occupancy of γ and $(\alpha+\beta)/2$, obtained by ARPES measurements (red dots and lines), and LDA calculations (black dots and lines).

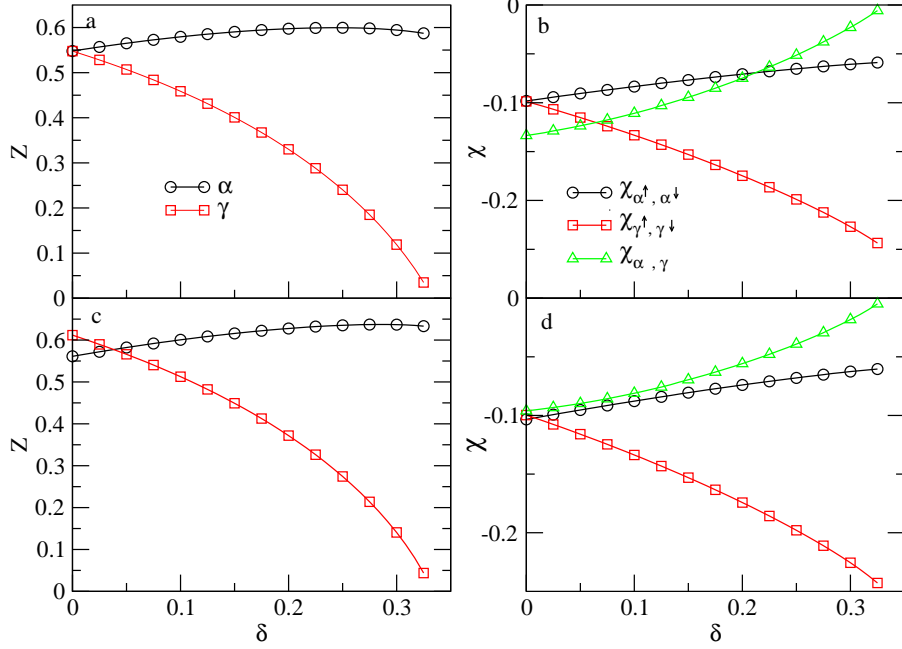


FIG. 4: **Calculations that show OSMT in multi-orbital systems** (a) The quasiparticle weight for the 3-band Hubbard model with equal bandwidth W as a function of charge transfer δ defined by $(n_\alpha, n_\beta, n_\gamma) = (\frac{2}{3} - \frac{\delta}{2}, \frac{2}{3} - \frac{\delta}{2}, \frac{2}{3} + \delta)$. $U/W=4.0$, $J/W=1.0$. (b) The intra-band and inter-band correlation functions, where $\chi_{\alpha^\uparrow, \alpha^\downarrow} = \langle n_{\alpha^\uparrow} n_{\alpha^\downarrow} \rangle - \langle n_{\alpha^\uparrow} \rangle \langle n_{\alpha^\downarrow} \rangle$, $\chi_{\gamma^\uparrow, \gamma^\downarrow} = \langle n_{\gamma^\uparrow} n_{\gamma^\downarrow} \rangle - \langle n_{\gamma^\uparrow} \rangle \langle n_{\gamma^\downarrow} \rangle$ and $\chi_{\alpha, \gamma} = \langle (n_{\alpha^\uparrow} + n_{\alpha^\downarrow})(n_{\gamma^\uparrow} + n_{\gamma^\downarrow}) \rangle - \langle (n_{\alpha^\uparrow} + n_{\alpha^\downarrow}) \rangle \langle (n_{\gamma^\uparrow} + n_{\gamma^\downarrow}) \rangle$. (c) Same as in panel A, except for the three bandwidths of $W, W, 1.5W$. (d) Same as in panel b, except for the three bandwidths of $W, W, 1.5W$. Note that the y-axis is negative in (b) and (d). With increasing δ , the intra γ -band correlation becomes large and negative, while the interband correlation approaches zero.